Supplement of Earth Syst. Sci. Data, 12, 1037–1051, 2020
https://doi.org/10.5194/essd-12-1037-2020-supplement


Open Access Earth System Science Data

*Supplement of*

# Spatial and temporal patterns of global soil heterotrophic respiration in terrestrial ecosystems

**Xiaolu Tang et al.**

*Correspondence to:* Shaohui Fan (fansh@icbr.ac.cn) and Wunian Yang (ywn@cdut.edu.cn)

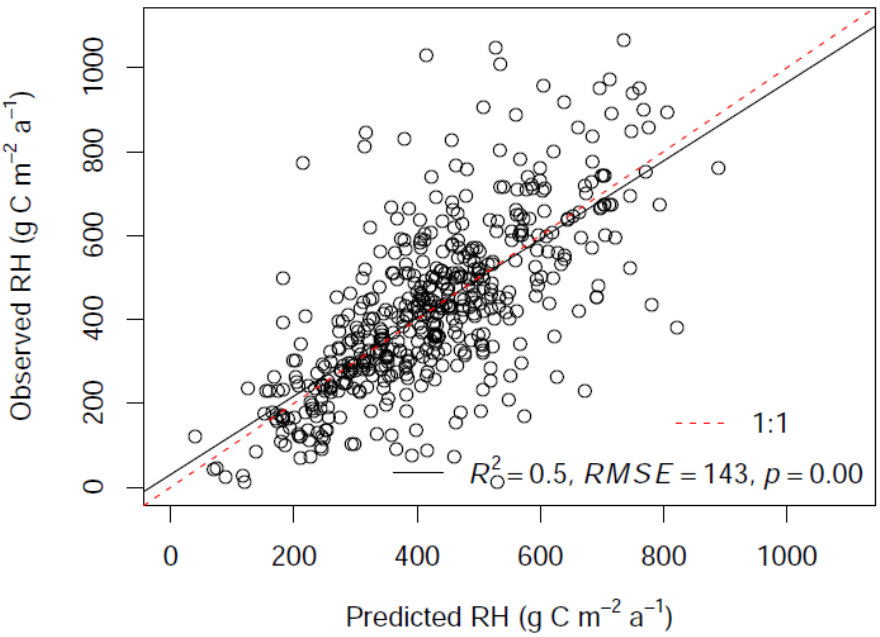


**Figure S1.** Comparison of observed soil heterotrophic respiration (RH) and predicted RH from Random Forest by 10-fold cross-validation.

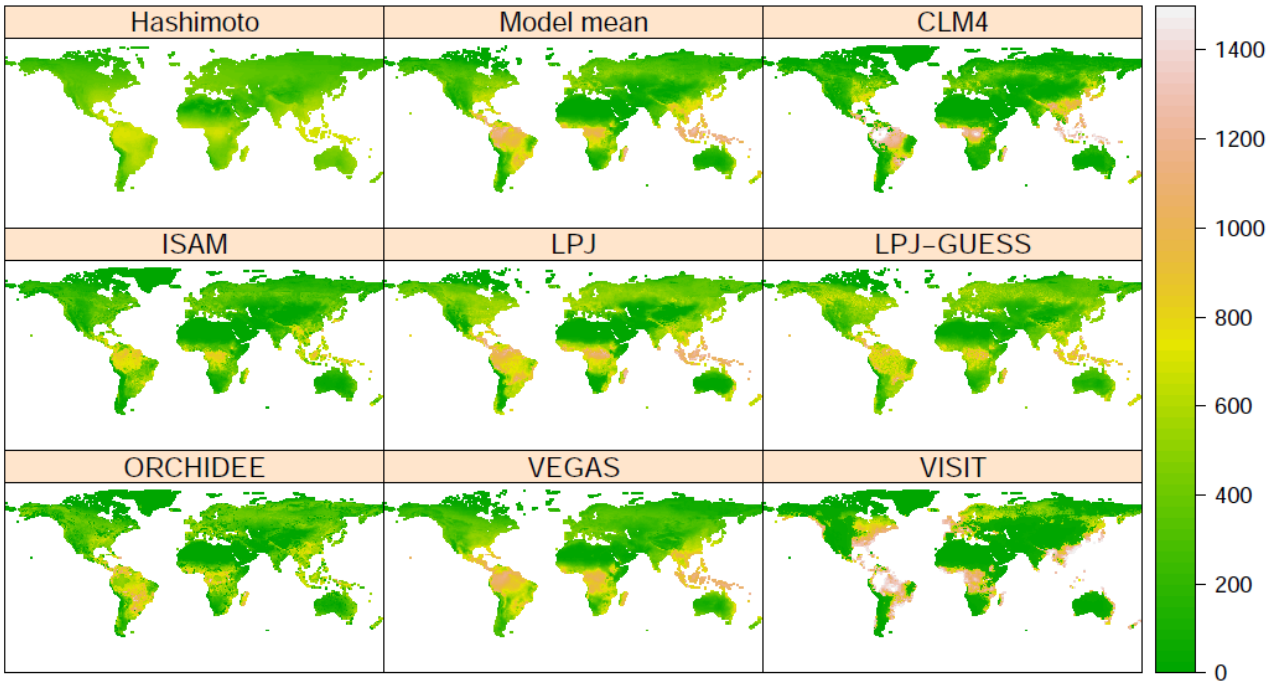


**Figure S2.** Spatial distribution for TRENDY/Hashimoto RH over 1981-2010

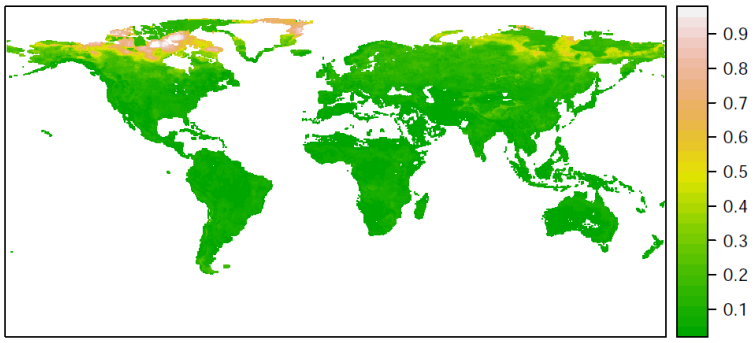


**Figure S3.** The uncertainty map (the ratio of standard deviation and mean value) of RH from 1980 to 2016 following Greaves et al. (2016).

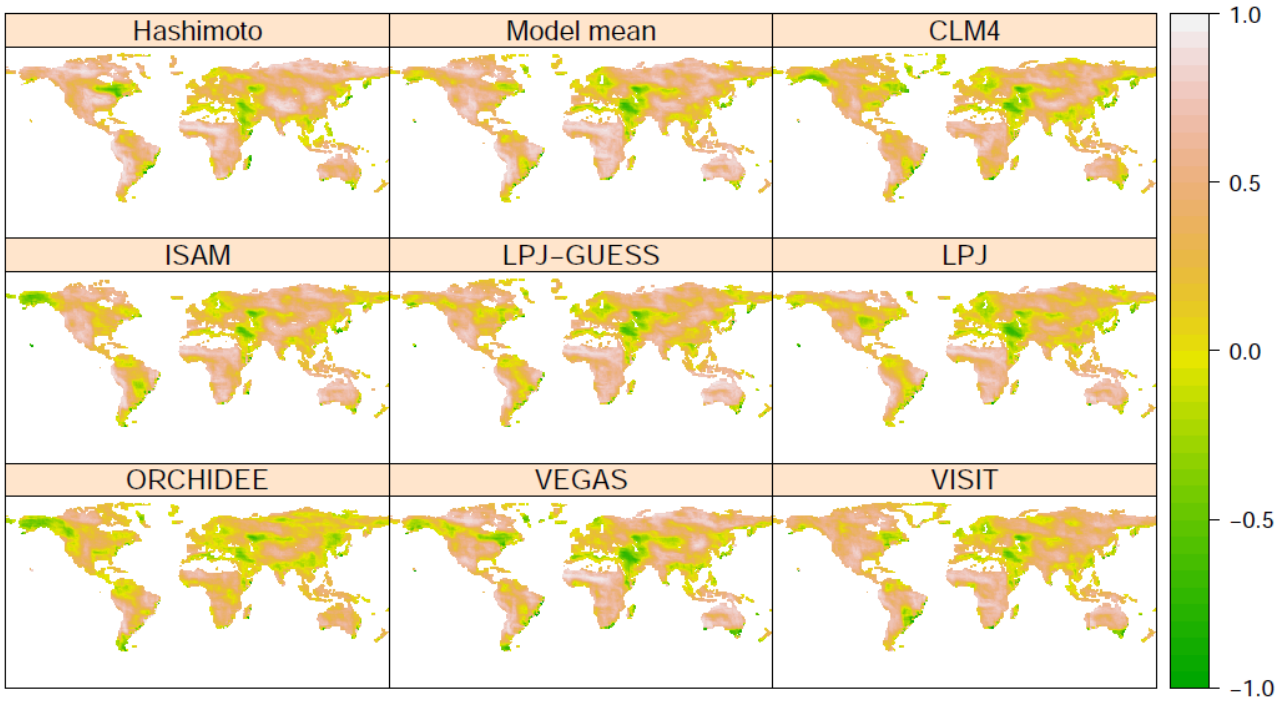


**Figure S4**. Cross-correlation between data-derived RH and TRENDY/Hashimoto RH

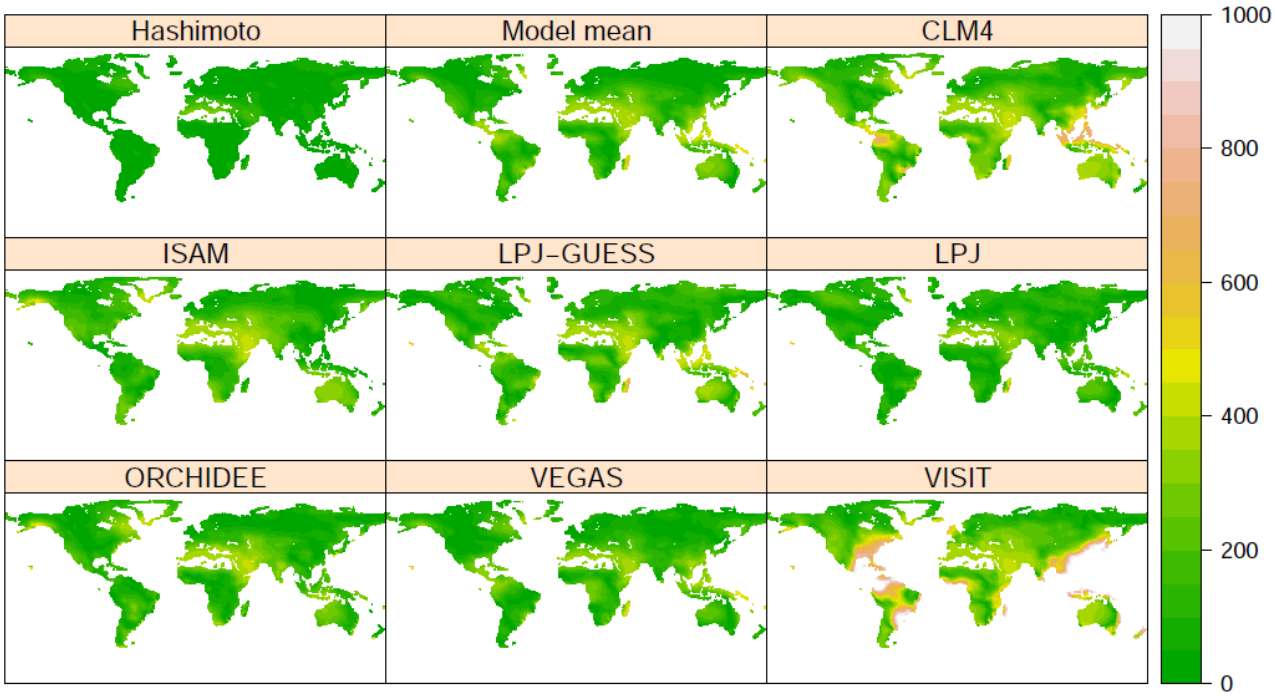


**Figure S5.** Absolute distance between data-derived RH and TRENDY/Hashimoto RH

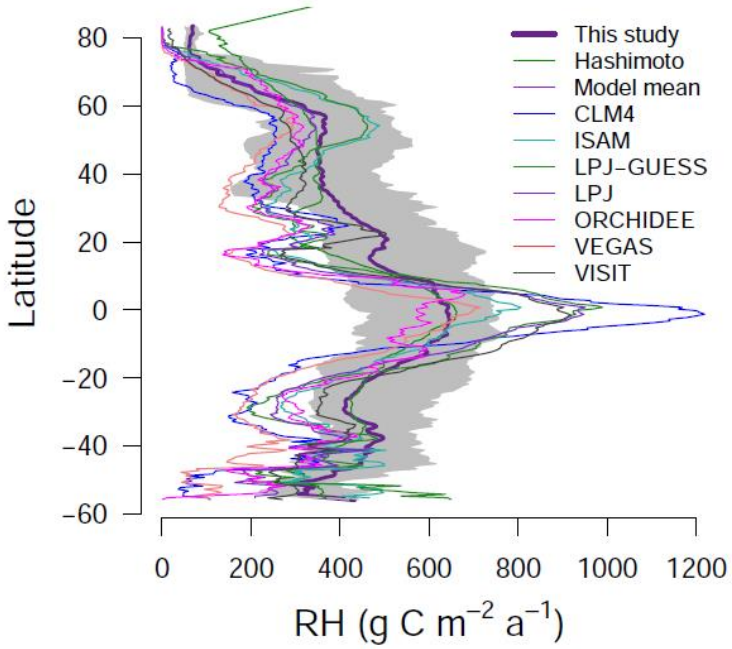


**Figure S6**. Latitudinal gradient of RH for data-derived product and TRENDY models. The grey range means 2.5 to 97.5 percentile ranges of the data-derived RH in this study.

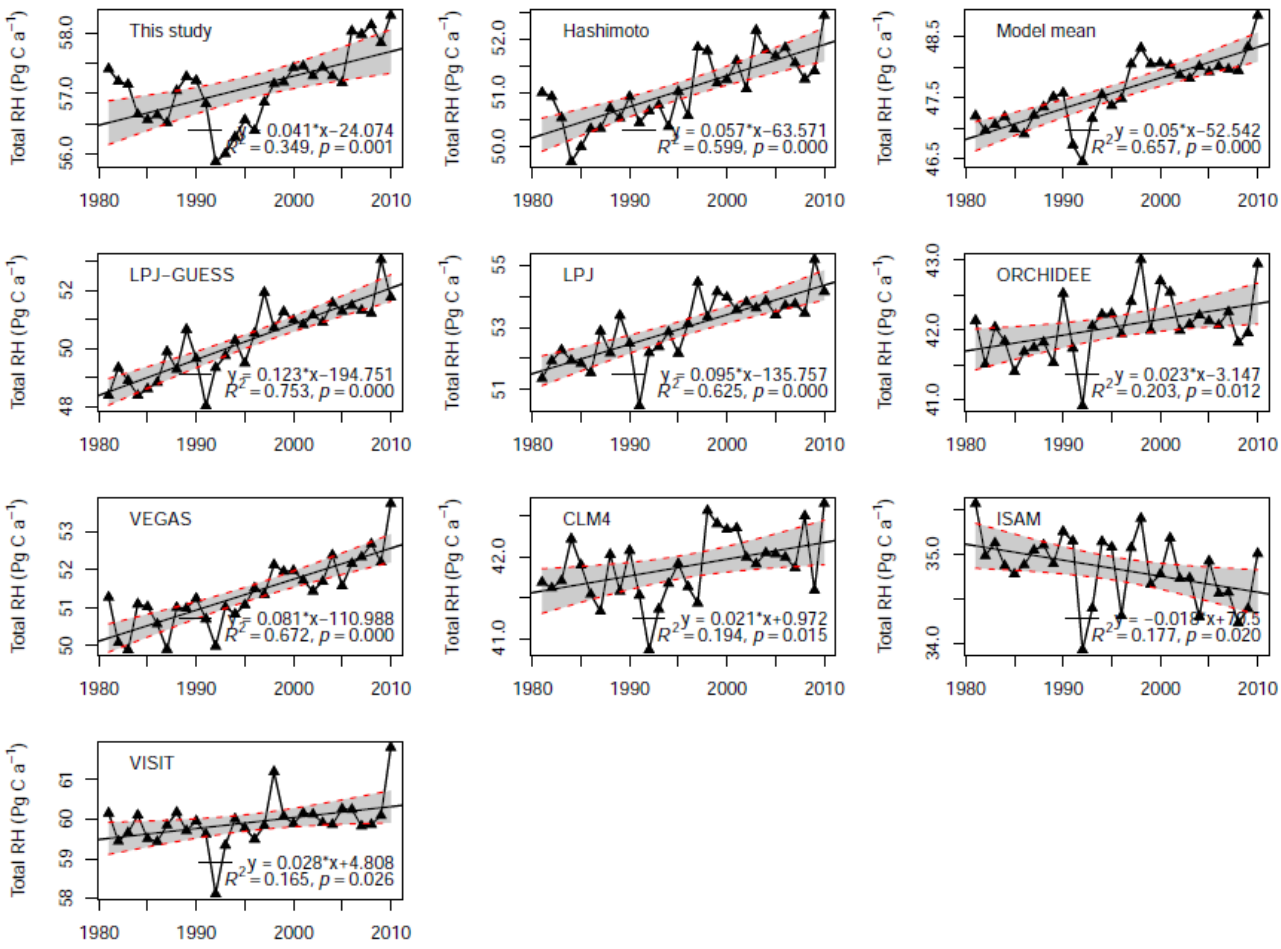


**Figure S7.** Temporal change of data-derived and TRENDY/Hashimoto RH from 1980 to 2010. The grey area indicates 95% confidence intervals.

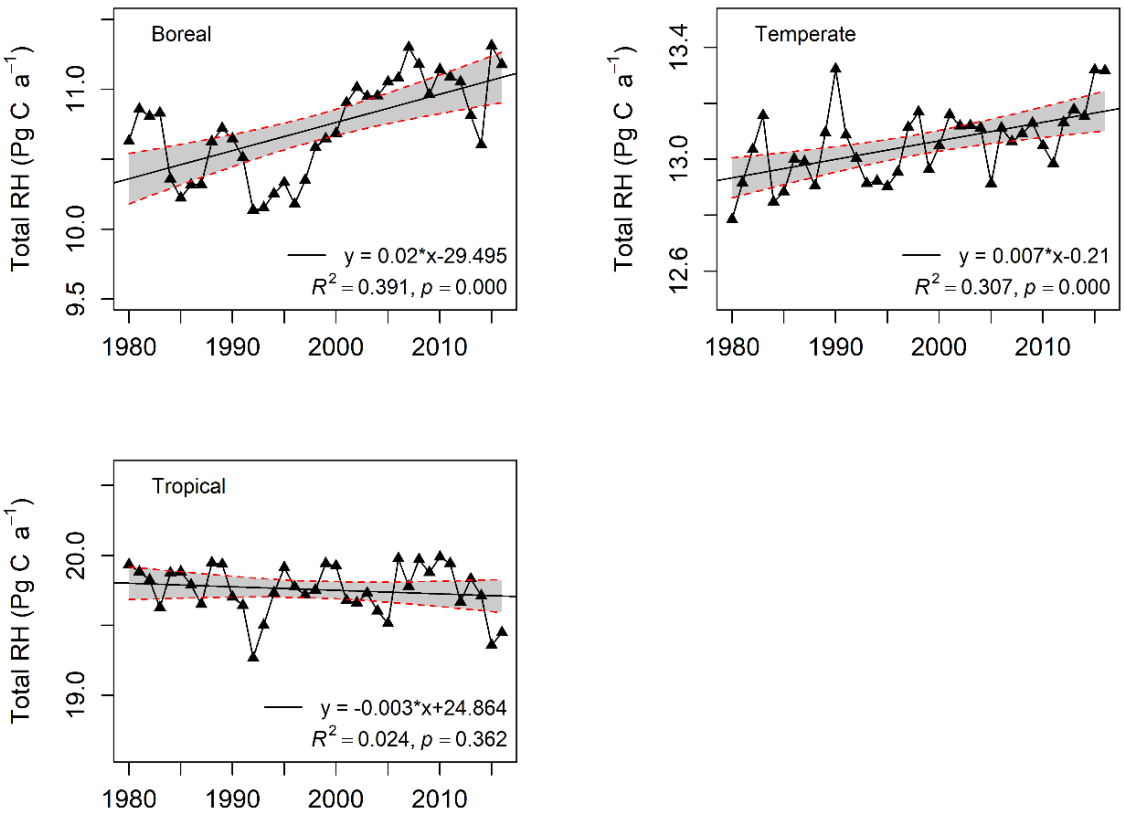


**Figure S8**. Annual change of data-derived RH for boreal, temperate and tropical areas from 1980 to 2016. The grey area indicates 95% confidence intervals.

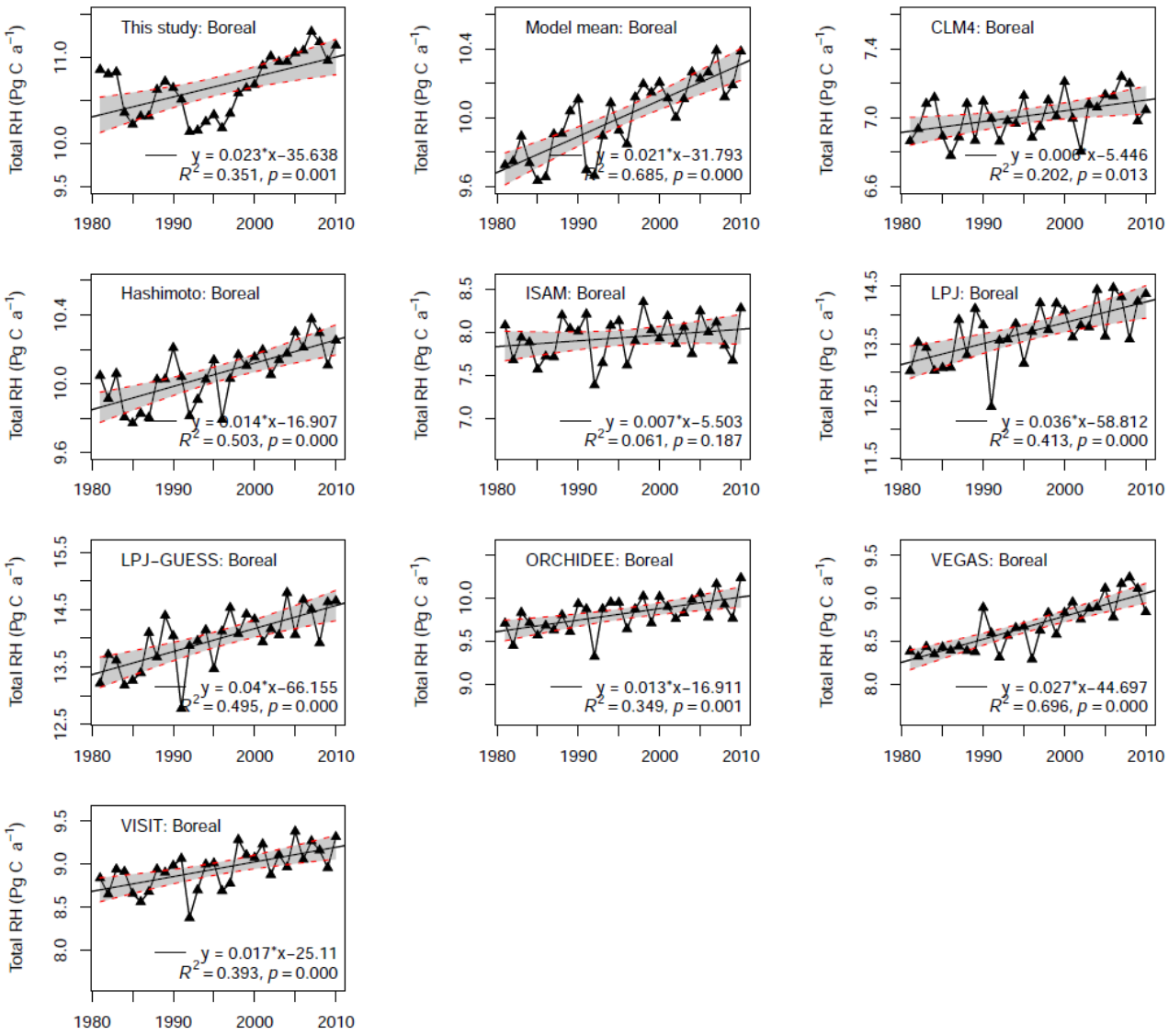


**Figure S9.** Annual change of TRENDY/Hashimoto RH for boreal areas. The grey area indicates 95% confidence intervals.

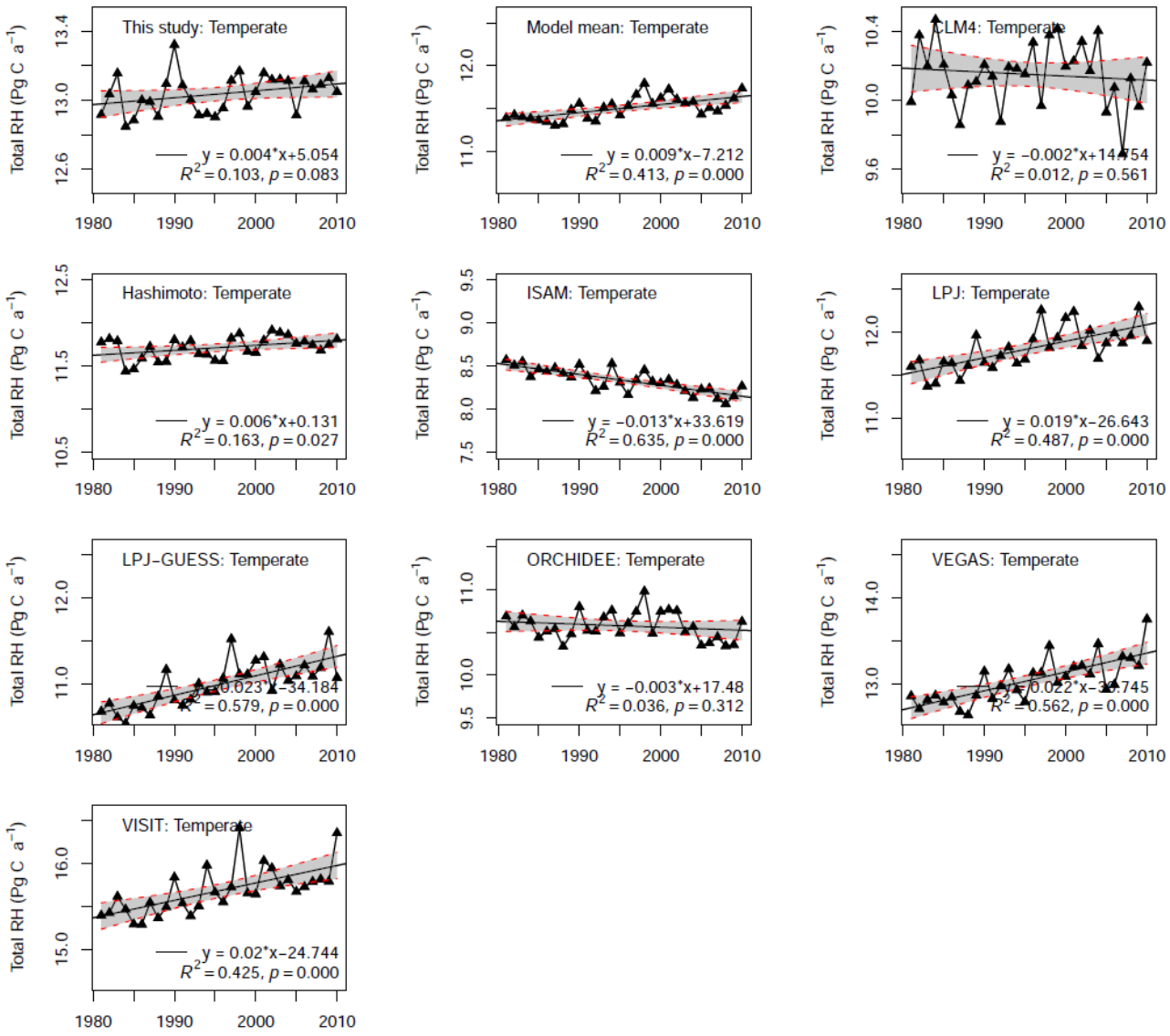


**Figure S10**. Annual change of TRENDY/Hashimoto RH for temperate areas. The grey area indicates 95% confidence intervals.

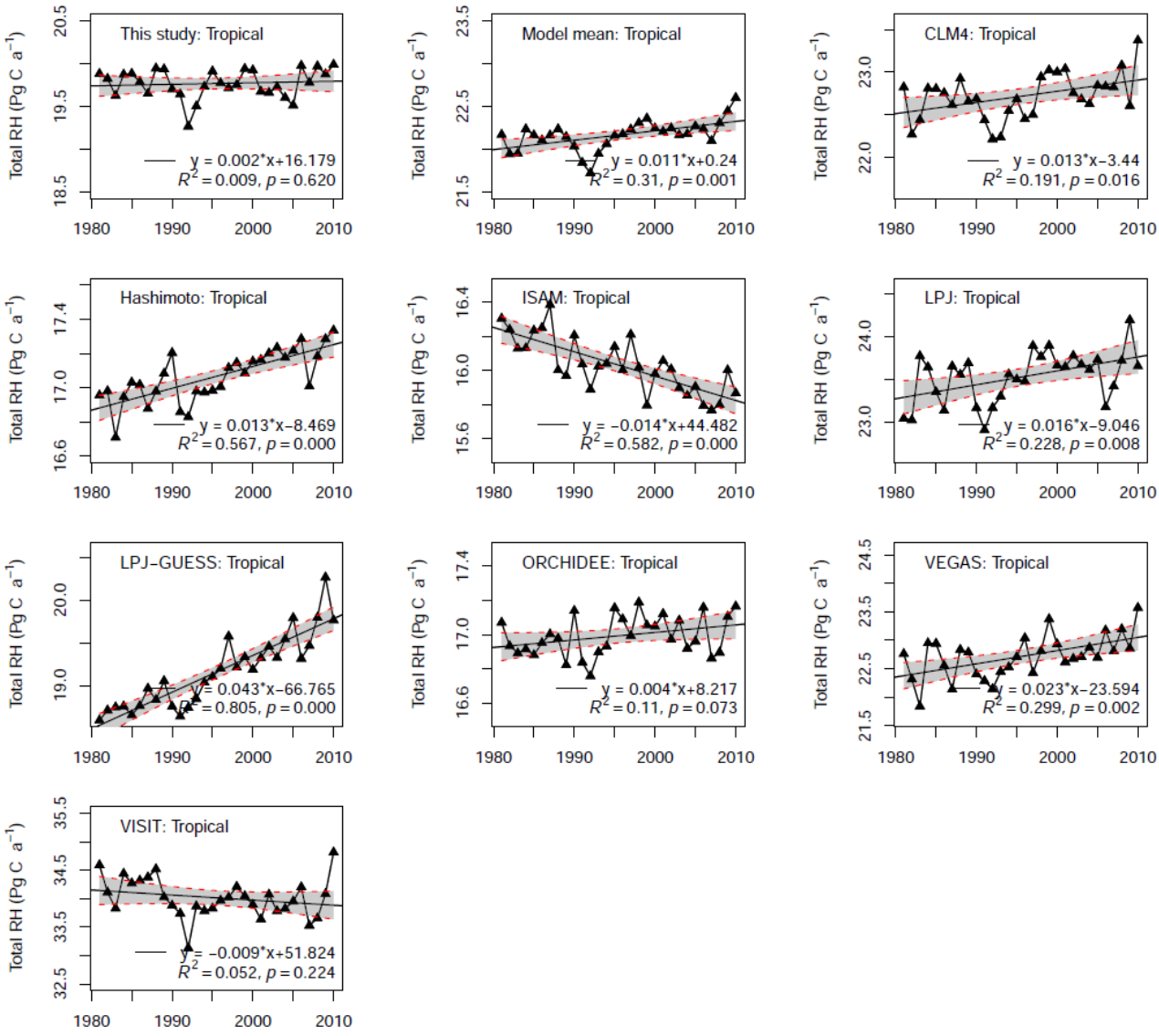


**Figure S11**. Annual change of TRENDY/Hashimoto RH for tropical areas. The grey area indicates 95% confidence intervals.

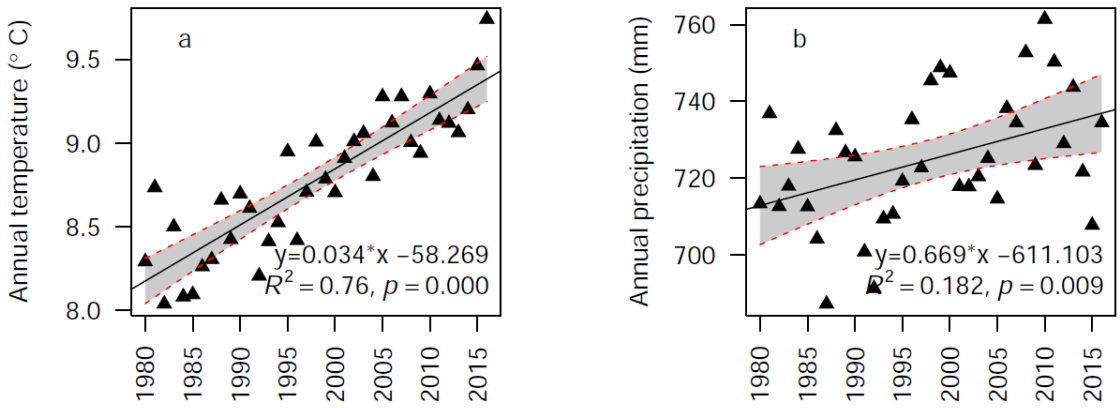


**Figure S12**. Temporal change of (a) global mean annual temperature, (b) precipitation. The grey area indicates 95% confidence intervals

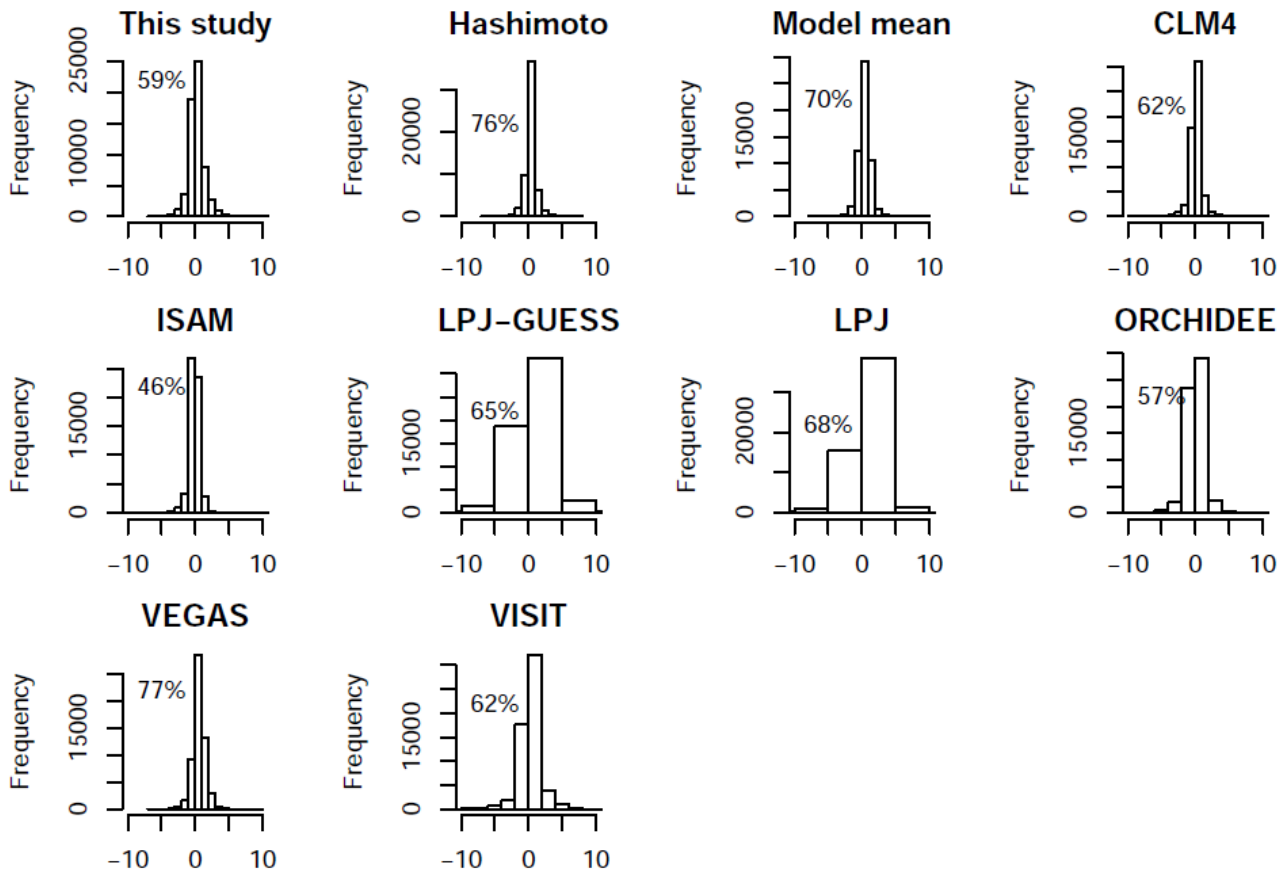


**Figure S13.** Frequency of temporal trend of data-derived RH, TRENDY/Hashimoto models. The percentages on the Figure indicated the increasing areas of RH within 1981-2010 for data-derived RH, Hashimoto, model mean and seven trendy models, respectively

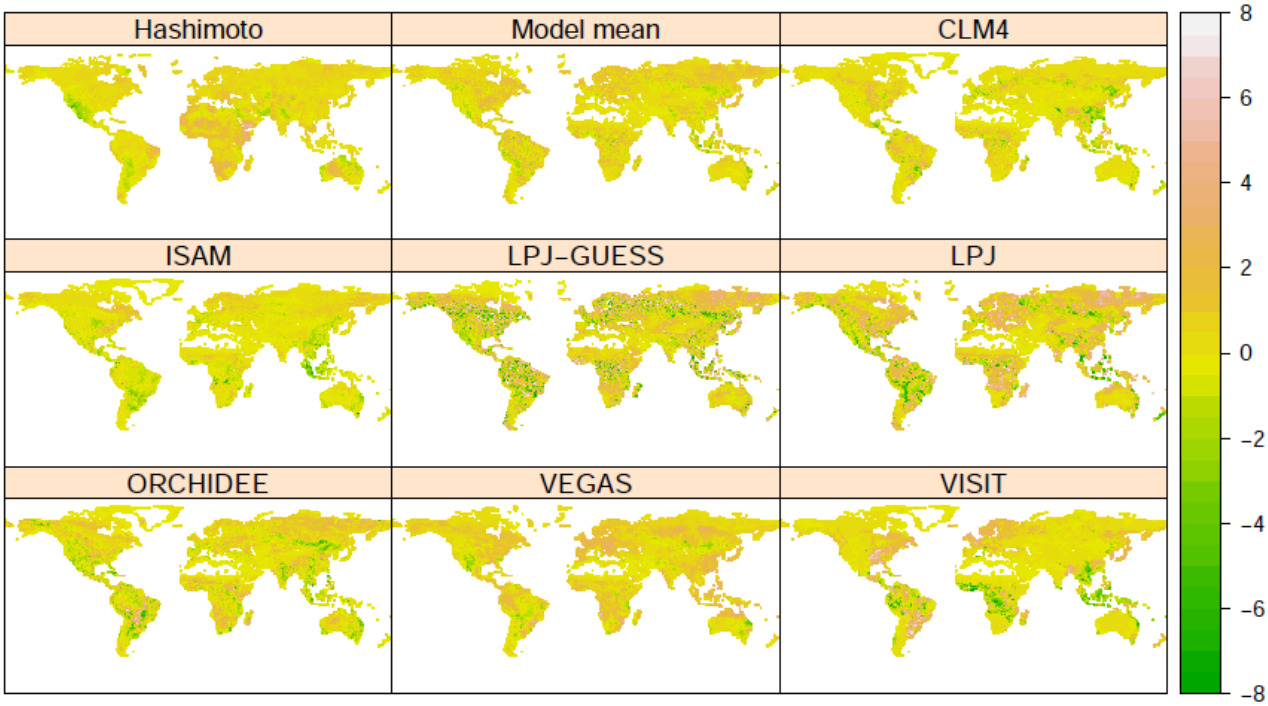


**Figure S14**. Spatial pattern in the trend of RH for TRENDY/Hashimoto models

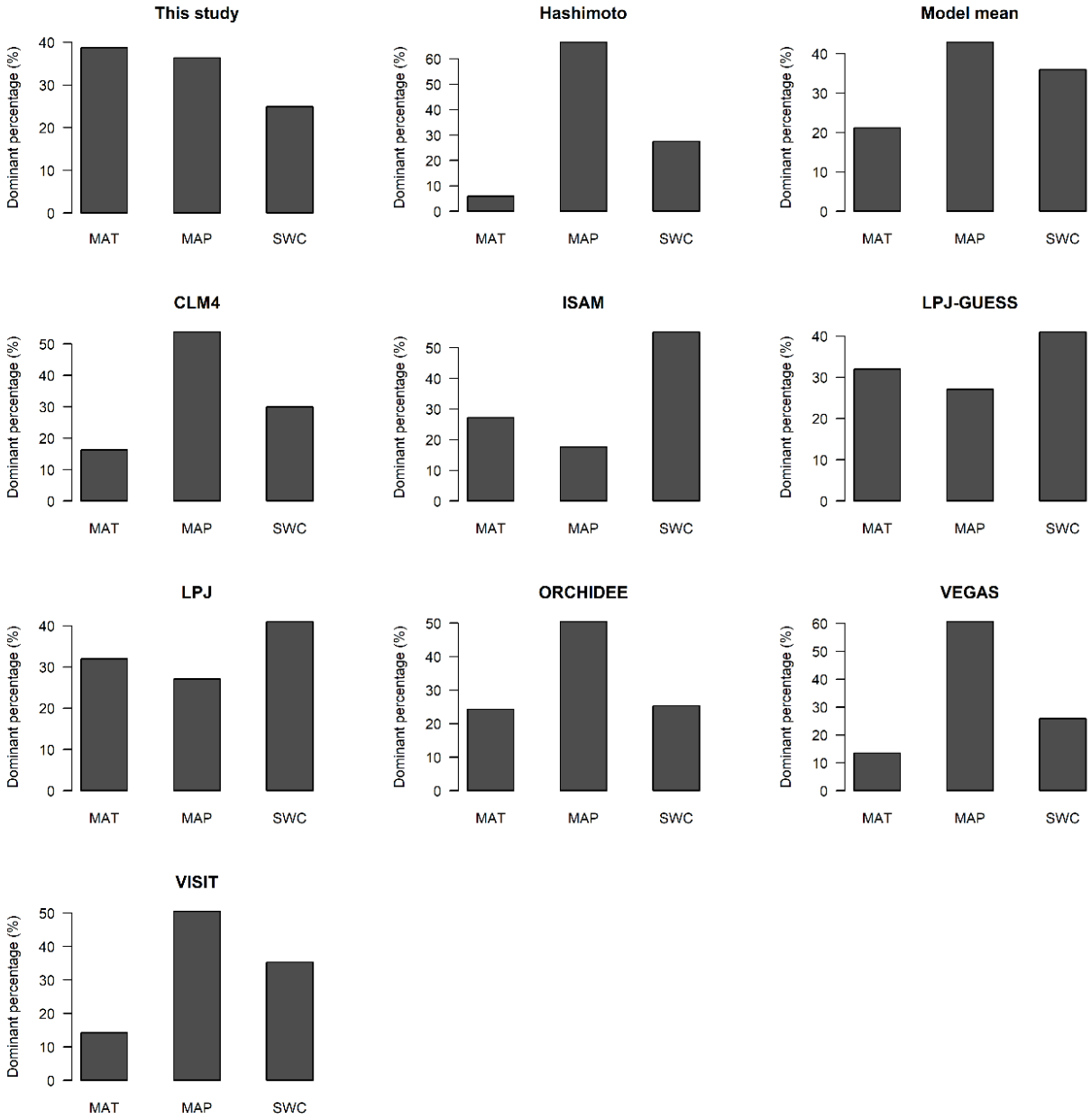


**Figure S15**. The percentage of areas dominated by temperature, precipitation and soil water content for Hashimoto/TRENDY RH

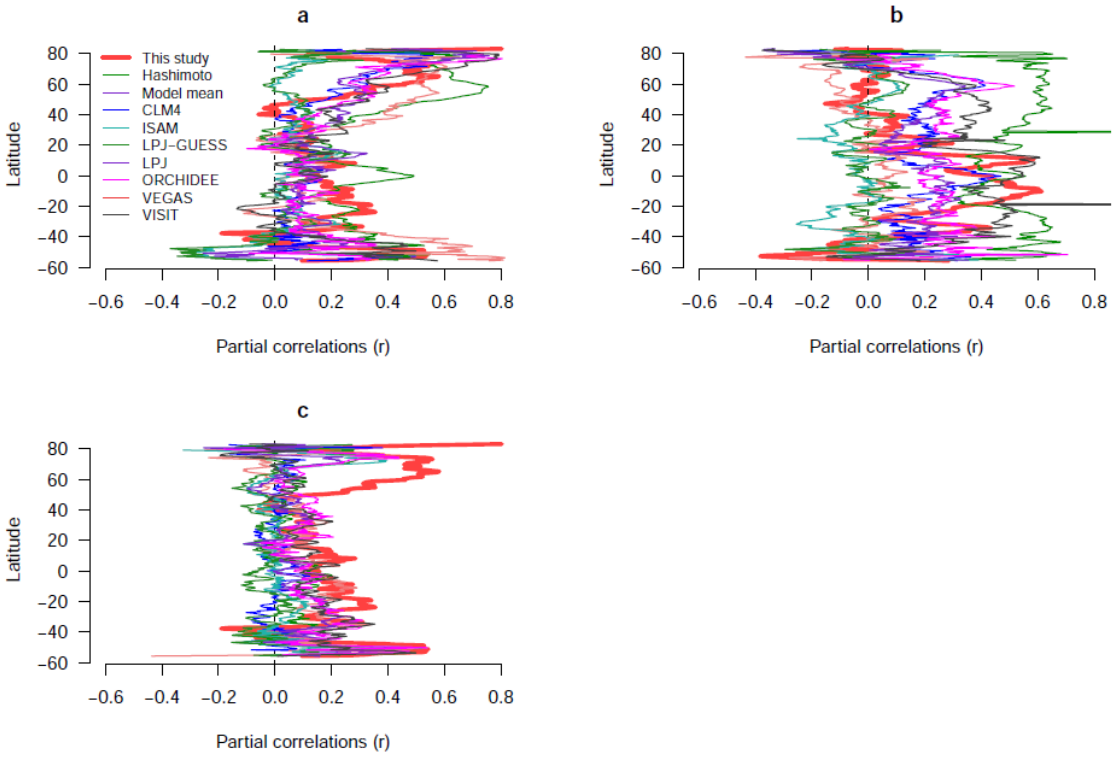


**Figure S16**. Latitudinal gradients of partial correlation coefficient between RH and (a) temperature, (b) precipitation and (c) soil water content. When analyzing the partial correlation between RH and the proxy, the other two proxies were controlled.

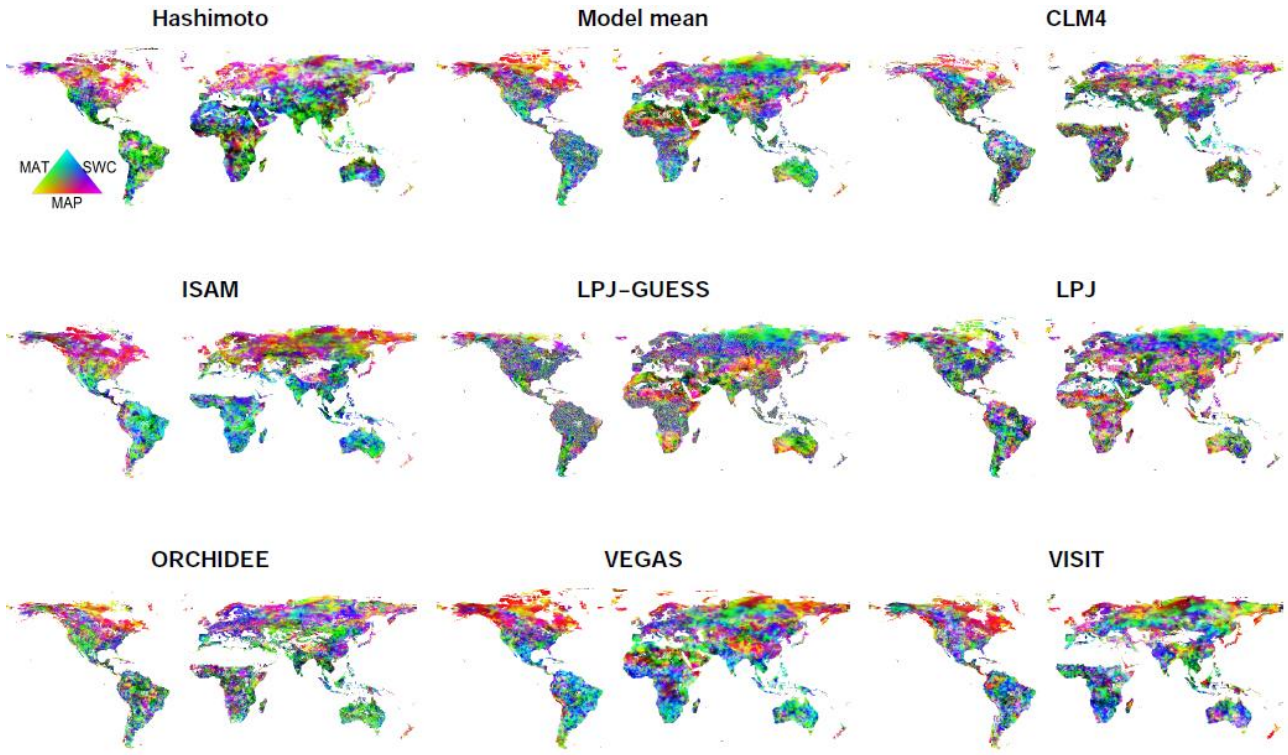


**Figure S17**. Environmental drivers for TRENDY/Hashimoto RH. MAT = mean annual temperature, MAP = mean annual precipitation, SWC = soil water content

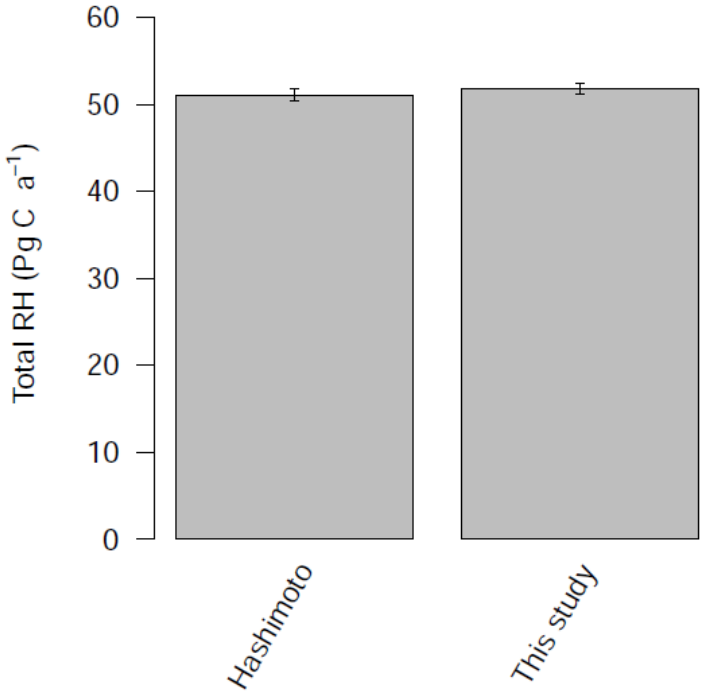


**Figure S18**. Global Hashimoto RH and data-derived RH in this study masked by Hashimoto RH. After masked for same land area, RH was 51.1 Pg C $a^{-1}$ for Hashimoto and 51.8 Pg C $a^{-1}$ for this study. The error bar means the standard deviation.

**Table S1.** Global variables used for predicting the temporal and spatial RH

| | Variables | Type | Type of variability | Sources |
|---|---|---|---|---|
| Climate | Mean annual temperature | Split | Yearly | https://crudata.uea.ac.uk/cru/data/hrg/cru_ts_4.01/ (Harris et al., 2014) |
| | Mean annual precipitation | Split | Yearly | |
| | Diurnal temperature range | Split | Yearly | |
| | Nitrogen deposition | Split | Yearly | https://www.isimip.org/gettingstarted/availability-input-data-isimip2b/ (Lamarque et al., 2013) |
| | Palmer Drought Severity Index | Split | Yearly | https://www.esrl.noaa.gov/psd/data/gridded/data.pdsi.html (Dai et al., 2004) |
| | Shortwave radiation | Split | Yearly | https://www.esrl.noaa.gov (Kalnay et l., 1996) |
| Soil | Soil carbon content | - | Static | https://soilgrids.org/#!/?layer=TAXNWRB_250m (Hengl et al., 2017) |
| | Soil nitrogen content | - | Static | https://webmap.ornl.gov/ogc/index.jsp (Global Soil Data, 2000) |
| | Soil water content | Split | Yearly | https://www.esrl.noaa.gov/psd/data/gridded/data.cpcsoil.html (van den Dool et al., 2003) |

## References


Dai, A., Trenberth, K. E., and Qian, T.: A Global Dataset of Palmer Drought Severity Index for 1870–2002: Relationship with Soil Moisture and Effects of Surface Warming, J. Hydrometeorol., 5, 1117-1130, http://dx.doi.org/10.1175/JHM-386.1, 2004.

Global Soil Data, T.: Global Gridded Surfaces of Selected Soil Characteristics (IGBP-DIS). ORNL Distributed Active Archive Center, http://dx.doi.org/10.3334/ornldaac/569, 2000.

Greaves, H. E., Vierling, L. A., Eitel, J. U. H., Boelman, N. T., Magney, T. S., Prager, C. M., and Griffin, K. L.: High-resolution mapping of aboveground shrub biomass in Arctic tundra using airborne lidar and imagery, Remote Sens. Environ., 184, 361-373, https://doi.org/10.1016/j.rse.2016.07.026, 2016.

Harris, I., Jones, P., Osborn, T., and Lister, D.: Updated high ‐ resolution grids of monthly climatic observations ‐ the CRU TS3. 10 Dataset, Int. J. Climatol., 34, 623-642, http://dx.doi.org/10.1002/joc.3711, 2014.

Hengl, T., Mendes de Jesus, J., Heuvelink, G. B., Ruiperez Gonzalez, M., Kilibarda, M., Blagotic, A., Shangguan, W., Wright, M. N., Geng, X., Bauer-Marschallinger, B., Guevara, M. A., Vargas, R., MacMillan, R. A., Batjes, N. H., Leenaars, J. G., Ribeiro, E., Wheeler, I., Mantel, S., and Kempen, B.: SoilGrids250m: Global gridded soil information based on machine learning, PLoS One, 12, e0169748, http://dx.doi.org/10.1371/journal.pone.0169748, 2017.

Kalnay, E., Kanamitsu, M., Kistler, R., Collins, W., Deaven, D., Gandin, L., Iredell, M., Saha, S., White, G., Woollen, J., Zhu, Y., Chelliah, M., Ebisuzaki, W., Higgins, W., Janowiak, J., Mo, K. C., Ropelewski, C., Wang, J., Leetmaa, A., Reynolds, R., Jenne, R., and Joseph, D.: The NCEP/NCAR 40-year reanalysis project, Bull. Am. Meteorol. Soc., 77, 437-471, http://dx.doi.org/10.1175/1520-0477(1996)077<0437:Tnyrp>2.0.Co;2, 1996.

Lamarque, J. F., Dentener, F., McConnell, J., Ro, C. U., Shaw, M., Vet, R., Bergmann, D., Cameron-Smith, P., Dalsoren, S., Doherty, R., Faluvegi, G., Ghan, S. J., Josse, B., Lee, Y. H., MacKenzie, I. A., Plummer, D., Shindell, D. T., Skeie, R. B., Stevenson, D. S., Strode, S., Zeng, G., Curran, M., Dahl-Jensen, D., Das, S., Fritzsche, D., and Nolan, M.: Multi-model mean nitrogen and sulfur deposition from the Atmospheric Chemistry and Climate Model Intercomparison Project (ACCMIP): evaluation of historical and projected future changes, Atmos. Chem. Phys., 13, 7997-8018, http://dx.doi.org/10.5194/acp-13-7997-2013, 2013.

van den Dool, H., Huang, J., and Fan, Y.: Performance and analysis of the constructed analogue method applied to U.S. soil moisture over 1981–2001, J. Geophys. Res. Atmos., 108, 8617, http://dx.doi.org/10.1029/2002jd003114, 2003.